A new formulation of fk for the PANS model

(article starts on next page)

Taylor & Francis
Taylor & Francis Group

A new formulation of f_k for the PANS model

Lars Davidson[a] and Christophe Friess[b]

[a]Division of Fluid Dynamics, Department of Mechanics and Maritime Sciences, Chalmers University of Technology, Gothenburg, Sweden; [b]Aix-Marseille Université, CNRS, Centrale Marseille, Marseille, M2P2, France

ABSTRACT

The partially averaged Navier–Stokes (PANS) model, proposed in Girimaji [Partially-averaged Navier-Stokes model for turbulence: a Reynolds-averaged Navier-Stokes to direct numerical simulation bridging method. ASME J Appl Mech. 2006;73(3):413–421], can be used to simulate turbulent flows either as a RANS, LES or DNS. The PANS model includes f_k which denotes the ratio of modelled to total kinetic energy. In RANS, $f_k = 1$, and in DNS it goes to zero. In the present study we propose a new formulation for f_k based on the H-equivalence introduced by Friess et al. [Toward an equivalence criterion for hybrid RANS/LES methods. Int J Heat Fluid Flow. 2015;122:233–246]. In this formulation the expression of f_k is derived to mimic DES. This new formulation behaves very much like classic DES, even though the two formulations use different mechanisms to separate modelled and resolved scales. They show very similar performance in separated flows as well as in attached boundary layers. Moreover, the new formulation exhibits similar robustness features as DES.

1. Introduction

The PANS model was proposed by Girimaji [1] and the PITM (Partially Integrated Transport Model) was proposed by Schiestel and Dejoan [2], Chaouat and Schiestel [3]. The critical parameter in both models is f_k (it is sometimes called r in PITM). It is defined as the ratio of the modelled to the total turbulent kinetic energy:

$$f_k = \frac{k}{k_{\text{tot}}}. \tag{1}$$

In DNS (Direct Numerical Solution), it tends to zero and in RANS (Reynolds-Averaged Navier–Stokes) it should be one. In LES (Large Eddy Simulation), the parameter takes values between zero and one. It is natural to link f_k to the mesh resolution and in that aim several proposals have been made on how to compute f_k. By seeking the smallest resolved length scale for a given f_k through dimensional analysis, Girimaji and Abdul-Hamid [4]

CONTACT L. Davidson ✉ lada@chalmers.se 🖥 Division of Fluid Dynamics, Department of Mechanics and Maritime Sciences, Chalmers University of Technology, SE-412 96 Gothenburg, Sweden

proposed one way to compute f_k:

$$f_k = C_\mu^{-1/2} \left(\frac{\Delta}{L_t} \right)^{2/3}, \quad L_t = \frac{k_{\text{tot}}^{3/2}}{\varepsilon} \tag{2}$$

using $\Delta = \Delta_{\min}$, the smallest grid cell size. Basara et al. also used f_k prescribed from Equation (2), however taking the geometric average $\Delta = (\Delta V)^{1/3}$. Kenjeres and Hanjalic [5] have made a slightly different proposal which reads

$$f_k = \frac{\Delta}{L_t} \tag{3}$$

Another way is to compute f_k from its very definition (1). k_{tot} is then computed using the running average. The expression (1) shall hereafter be refered to as $f_{k,\text{obs}}$, the *observed* f_k. More recently, Foroutan and Yavuzkurt [6] derived an expression from the Kolmogorov energy spectrum which reads

$$f_k = 1 - \left[\frac{(\Lambda/\Delta)^{2/3}}{0.23 + (\Lambda/\Delta)^{2/3}} \right]^{9/2}. \tag{4}$$

In [7], the expression in Equation (3) was found to give far too small f_k. The form in Equation (2) and (1) were evaluated but it was found that a constant $f_k = 0.4$ in the LES region is superior.

The present paper is based on the work in [8] where they derived a relation between DES and PITM. They showed that the DES model could be formulated using f_k. They call this model an equivalent DES model. The relation between DES and PANS is used in the present work, but it is used the other way around: a new form of f_k is derived based on the DES model. In [9] the form of f_k (new PANS, detailed in Section 2.1) was compared to DES. and the two models were found to give more or less identical results, particularly regarding first-order moments: velocity, skin friction coefficient C_f. In the present work the new PANS will be compared to the expression in Equation (2) (the old PANS using $\Delta = (\Delta V)^{1/3}$) which in the literature is the most common way to compute f_k.

The paper is organised as follows. First, the form of f_k is derived and analysed analytically. In the following section we present the numerical method. Then the new and old PANS are compared in three different flows (channel flow, hump flow and hill flow). Some conclusions are drawn in the final section.

2. The PANS model

The low-Reynolds number Partially-Averaged Navier–Stokes (LRN PANS, see [10]) turbulence model reads

$$\frac{dk}{dt} = \frac{\partial}{\partial x_j} \left[\left(\nu + \frac{\nu_t}{\sigma_{ku}} \right) \frac{\partial k}{\partial x_j} \right] + P_k - \varepsilon$$

$$\frac{d\varepsilon}{dt} = \frac{\partial}{\partial x_j} \left[\left(\nu + \frac{\nu_t}{\sigma_{\varepsilon u}} \right) \frac{\partial \varepsilon}{\partial x_j} \right] + C_{\varepsilon 1} P_k \frac{\varepsilon}{k} - C_{\varepsilon 2}^* \frac{\varepsilon^2}{k}$$

$$\nu_t = C_\mu f_\mu \frac{k^2}{\varepsilon}, \quad P_k = 2\nu_t \bar{s}_{ij} \bar{s}_{ij}, \quad \bar{s}_{ij} = \frac{1}{2} \left(\frac{\partial \bar{v}_i}{\partial x_j} + \frac{\partial \bar{v}_j}{\partial x_i} \right) \tag{5}$$

$$C_{\varepsilon 2}^* = C_{\varepsilon 1} + \frac{f_k}{f_\varepsilon}(C_{\varepsilon 2}f_2 - C_{\varepsilon 1}), \quad \sigma_{ku} \equiv \sigma_k \frac{f_k^2}{f_\varepsilon}, \quad \sigma_{\varepsilon u} \equiv \sigma_\varepsilon \frac{f_k^2}{f_\varepsilon}$$

$$\sigma_k = 1.4, \quad \sigma_\varepsilon = 1.4, \quad C_{\varepsilon 1} = 1.5, \quad C_{\varepsilon 2} = 1.9, \quad C_\mu = 0.09,$$

where $d/dt = \partial/\partial t + \bar{v}_j \partial/\partial x_j$ denotes the material derivative. The damping functions are given by

$$f_2 = \left[1 - \exp\left(-\frac{y^*}{3.1}\right)\right]^2 \left\{1 - 0.3\exp\left[-\left(\frac{R_t}{6.5}\right)^2\right]\right\}$$

$$f_\mu = \left[1 - \exp\left(-\frac{y^*}{14}\right)\right]^2 \left\{1 + \frac{5}{R_t^{3/4}}\exp\left[-\left(\frac{R_t}{200}\right)^2\right]\right\}$$

$$R_t = \frac{k^2}{\nu\varepsilon}, \quad y^* = \frac{U_\varepsilon y}{\nu}, \quad U_\varepsilon = (\varepsilon\nu)^{1/4}. \tag{6}$$

The functions f_k and f_ε denote the ratio of modelled to total kinetic energy and modelled to total dissipation, respectively. For flows at high Reynolds numbers (as in the present work), the dissipation is modelled which means that $f_\varepsilon = 1$. In the PITM model, $\sigma_{ku} \equiv \sigma_k$ and $\sigma_{\varepsilon u} \equiv \sigma_\varepsilon$.

2.1. f_k derived from the equivalence criterion

In [8] a relation between f_k and the grid step is derived, through the establishment of a statistical equivalence between DES and PITM. To that aim, they performed perturbation analyses about the equilibrium states, representing small variation of the energy partition. They did the analysis with and without considering inhomogeneity. That derivation is summarised here in a homogeneous framework, as a first step. Let us first consider the PANS/PITM equations. For equilibrium turbulence $d\tau/dt = 0$ where $\tau = k/\varepsilon$, Equation (5) gives

$$\frac{d\tau}{dt} = \frac{1}{\varepsilon}\frac{dk}{dt} - \frac{k}{\varepsilon^2}\frac{d\varepsilon}{dt} = \frac{1}{\varepsilon}\left(P^k + D^k - \varepsilon\right)$$

$$- \frac{k}{\varepsilon^2}\left(C_{\varepsilon 1}\frac{\varepsilon}{k}P^k + D^\varepsilon - C_{\varepsilon 2}^*\frac{\varepsilon^2}{k}\right) = 0, \tag{7}$$

where D^k and D^ε denote the diffusion term for k and ε, respectively. For local homogeneous turbulence (i.e. $D^k = D^\varepsilon = 0$), it can be written

$$\gamma(C_{\varepsilon 1} - 1)Sk = (C_{\varepsilon 2}^* - 1)\varepsilon$$

$$\gamma = \frac{P^k}{Sk}, \quad S = (2\bar{s}_{ij}\bar{s}_{ij})^{1/2}. \tag{8}$$

The quantities that are affected by the partition between modelled and resolved turbulence (i.e. f_k) in Equation (8) are γ, S, k and $C_{\varepsilon 2}^*$.[1] Differentiation of Equation (8), by considering

infinitesimal perturbations $\delta\gamma$, δS, δk and $\delta C^*_{\varepsilon 2}$ of the variables, yields:

$$\delta\gamma Sk + \delta S\gamma k + \delta k\gamma S = \frac{\delta C^*_{\varepsilon 2}\varepsilon}{C_{\varepsilon 1} - 1} \tag{9}$$

so that

$$\frac{\delta\gamma}{\gamma} + \frac{\delta S}{S} + \frac{\delta k}{k} = \frac{\delta C^*_{\varepsilon 2}\varepsilon}{(C_{\varepsilon 1} - 1)\gamma Sk} = \frac{\delta C^*_{\varepsilon 2}}{C^*_{\varepsilon 2} - 1}. \tag{10}$$

Equation (10) was derived for the PANS/PITM equations. Now we repeat the derivation for the DES equations. The differences between DES and PITM/PANS are that in DES (i) $C^*_{\varepsilon 2} = C_{\varepsilon 2}$ is constant and (ii) the dissipation term in the equation for modelled energy k is replaced with $\psi\varepsilon$, i.e.

$$\frac{\mathrm{d}k}{\mathrm{d}t} = \frac{\partial}{\partial x_j}\left[\left(\nu + \frac{\nu_t}{\sigma_k}\right)\frac{\partial k}{\partial x_j}\right] + P_k - \psi\varepsilon \tag{11}$$

$$\psi = \max\left(1, \frac{k^{3/2}/\varepsilon}{C_{DES}\Delta_{\max}}\right), \quad \Delta_{\max} = \max(\Delta x_1, \Delta x_2, \Delta x_3)$$

$$\frac{\mathrm{d}\varepsilon}{\mathrm{d}t} = \frac{\partial}{\partial x_j}\left[\left(\nu + \frac{\nu_t}{\sigma_\varepsilon}\right)\frac{\partial\varepsilon}{\partial x_j}\right] + C_{\varepsilon 1}P_k\frac{\varepsilon}{k} - C_{\varepsilon 2}\frac{\varepsilon^2}{k}. \tag{12}$$

Assuming $\mathrm{d}\tau/\mathrm{d}t = 0$ and local homogeneous turbulence gives

$$\gamma(C_{\varepsilon 1} - 1)Sk = (C_{\varepsilon 2} - \psi)\varepsilon. \tag{13}$$

We differentiate so that

$$\frac{\delta\gamma}{\gamma} + \frac{\delta S}{S} + \frac{\delta k}{k} = -\frac{\mathrm{d}\psi\varepsilon}{(C_{\varepsilon 1} - 1)Sk\gamma} = -\frac{\mathrm{d}\psi}{C_{\varepsilon 2} - \psi}. \tag{14}$$

Equations (9) and (14) describe how $C^*_{\varepsilon 2}$ and ψ depend on variations in γ, S and k. The parameters $C^*_{\varepsilon 2}$ and ψ vary from $C_{\varepsilon 2}$ and 1 (RANS values), respectively, to $C^*_{\varepsilon 2}$ and $\psi(\Delta)$ (LES values). Combining Equations (9) and (14) and integrating from RANS to LES conditions ($C^*_{\varepsilon 2}$ and ψ)

$$\int_{C_{\varepsilon 2}}^{C^*_{\varepsilon 2}} \frac{\mathrm{d}C^*_{\varepsilon 2}}{C^*_{\varepsilon 2} - 1} = \int_1^\psi -\frac{\mathrm{d}\psi}{C_{\varepsilon 2} - \psi} \Rightarrow \ln\left(\frac{C^*_{\varepsilon 2} - 1}{C_{\varepsilon 2} - 1}\right) = \ln\left(\frac{C_{\varepsilon 2} - \psi}{C_{\varepsilon 2} - 1}\right). \tag{15}$$

By using the expression for $C^*_{\varepsilon 2}$ in Equation (5) (with $f_2 = f_\varepsilon = 1$), and ensuring that $0 < f_k \leq 1$ we finally get

$$f_k = \max\left[0, \min\left(1, 1 - \frac{\psi - 1}{C_{\varepsilon 2} - C_{\varepsilon 1}}\right)\right], \tag{16}$$

where ψ is given by Equation (12). This may be compared with the old formulations in Equations (2), (3) and (4). However, the present study focuses on a comparison between Equations (2) and (16).

2.2. Self-adaptivity properties of the new formulation of f_k for PANS

In this section, we will distinguish $f_{k,\text{obs}}$ (see Equation (1)), the *observed* energy ratio, from $f_{k,\text{tar}}$, the *targeted* (or prescribed) energy ratio. In the turbulent closure equations (i.e.in PANS, computing $C_{\varepsilon 2}^*$), $f_{k,\text{tar}}$ is used, but nothing ever guarantees that this level of modelled energy will be exactly reached, see e.g. [11]. This can be explained by the fact that $f_{k,\text{tar}}$ is a rough estimate, obtained under assumptions that are not always fully valid. Meanwhile, $f_{k,\text{obs}}$ can be obtained from postprocessing, using its definition in Equation (1).

If the targeted energy ratio, $f_{k,\text{tar}}$, is computed following Equation (16), and if we use the definition (which is rigorous in average)

$$k \simeq f_{k,\text{obs}}k_{\text{tot}}, \quad \text{where } k_{\text{tot}} = \langle k \rangle + \langle k_{\text{res}} \rangle \tag{17}$$

and the assumption that the whole dissipation is modelled, i.e. $f_\varepsilon = 1$ (at high Reynolds number):

$$\varepsilon \approx \varepsilon_{\text{tot}}, \tag{18}$$

then Equation (16) can be rewritten as:

$$f_{k,\text{tar}} = 1 - \frac{1}{C_{\varepsilon 2} - C_{\varepsilon 1}} \left[\max \left(1, \frac{f_{k,\text{obs}}^{3/2}}{C_{\text{DES}}\Delta_{\max}} \frac{k_{\text{tot}}^{3/2}}{\varepsilon_{\text{tot}}} \right) - 1 \right]. \tag{19}$$

(note that, for sake of clarity, the form of $f_{k,\text{tar}}$ is here allowed to go negative). This implies that $f_{k,\text{tar}}$ is implicitly linked to $f_{k,\text{obs}}$, in the following way: if $f_{k,\text{obs}}$ is lower (resp. higher) than a certain threshold value, $f_{k,\text{tar}}$ will increase (resp. decrease), leading dynamically to an increase (resp. decrease) of k and thus $f_{k,\text{obs}}$.

Of course, this rough reasoning assumes that the resolved part of k 'responds' to those changes quickly enough to leave k_{tot} almost unaffected.

Thus, one can conclude that defining $f_{k,\text{tar}}$ according to Equation (16) drives $f_{k,\text{obs}}$ towards a certain threshold (which may be more or less close to $f_{k,\text{tar}}$). Such a feature is not intrinsic to approaches such as PITM or PANS, if some spectral law or Equations (2), (3) or (4) are used to determine $f_{k,\text{tar}}$. It is actually intrinsic to Detached Eddy Simulation (DES), from which the present new formulation of f_k inherits this interesting property. This strategy may be interpreted as passive control, since it does not require the explicit computation of any extra quantity, such as $f_{k,\text{obs}}$.

3. Numerical solver

An incompressible, finite volume code is used [12]. The convective terms in the momentum equations are discretised using central differencing. Hybrid central/upwind is used for the k and ε equations. The Crank–Nicolson scheme is used for time discretisation of all equations. The numerical procedure is based on an implicit, fractional step technique with a multigrid pressure Poisson solver [13] and a non-staggered grid arrangement.
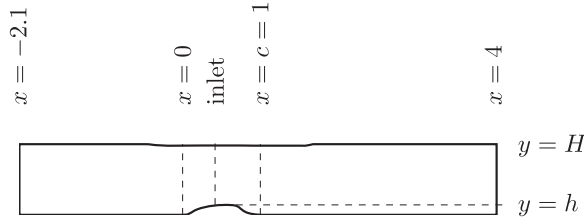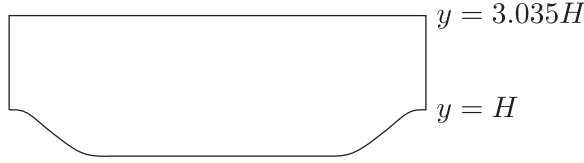
Figure 1. The geometry of the hump.

Figure 2. The geometry of the hill.

The filtered momentum equations with an added turbulent viscosity read

$$\frac{\partial \bar{v}_i}{\partial t} + \frac{\partial \bar{v}_j \bar{v}_i}{\partial x_j} = \beta \delta_{1i} - \frac{1}{\rho}\frac{\partial \bar{p}}{\partial x_i} + \frac{\partial}{\partial x_j}\left((v + v_t)\frac{\partial \bar{v}_i}{\partial x_j}\right), \tag{20}$$

where the first term on the right side is the driving pressure gradient in the streamwise direction, which is used in the fully-developed channel flow simulations and for the hill flow.

4. Results

The new formulation of f_k is evaluated and compared with the old formulation given in Equation (2). Herafter, they will be referred to as 'new PANS' and 'old PANS'. The comparison is performed in three test cases: fully developed channel flow, the hump flow (see Figure 1), and the hill flow (see Figure 2).

Ensemble-averaged quantities are plotted hereafter, i.e. they are averaged in time and over statistically homogeneous directions (which differ with flow cases).

4.1. Channel flow

The Reynolds number is defined as $Re_\tau = u_\tau \delta / v = 5200$ where δ denotes half channel height and u_τ is the friction velocity. The streamwise, wall-normal and spanwise directions are denoted by x, y and z, respectively. The size of the domain is $x_{max} = 3.2$, $y_{max} = 2$ and $z_{max} = 1.6$. The mesh has $32 \times 96 \times 32$ cells in the $x−y−z$ directions. Periodic boundary conditions are used in the x and z directions. Therefore, these two directions are considered statistically homogeneous. A precursor DES computation is used as initial condition. The driving pressure gradient (first term on the right-hand side in Equation (20) is used with $\beta = 1$. A lower limit of 0.05 is used when computing f_k from Equation (16).

Figure 3 presents the mean velocity and the turbulent kinetic energy profiles. As can be seen, the new PANS exhibits a small bump near $y^+ = 1000$; otherwise it agrees well with
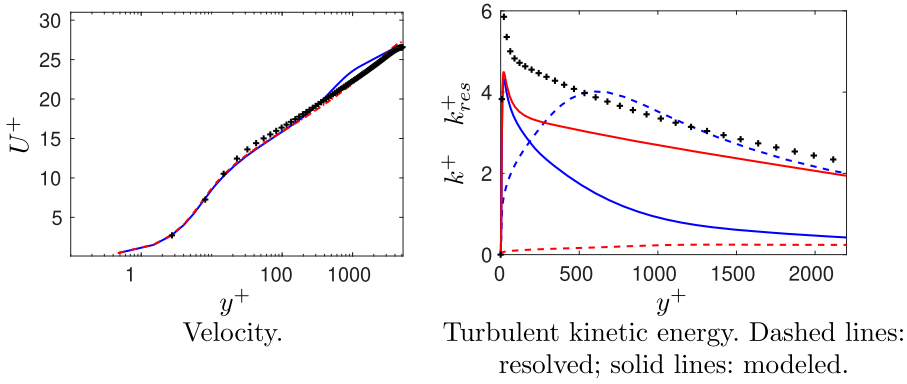
Figure 3. Channel flow, $Re_\tau = 5200$. Blue lines: new PANS; red lines: old PANS, see Equation (2) $Re_\tau = 5200$. Markers: DNS [14].

the DNS profile. The predicted turbulent kinetic energies with both old and new PANS agree well with DNS for $y^+ \gtrsim 500$. However, there is a big difference in how much turbulence is resolved and how much is modelled. For $y^+ \gtrsim 500$, all turbulence is resolved by the new PANS model. In the old PANS model, all turbulence is modelled. The reason is found in Figure 4(b)): the old PANS predicts $f_k \simeq 1$ in the entire region which means that the model is working in RANS mode. This is also seen in Figure 4(a)) in which it can be seen that the turbulent viscosity predicted by the old PANS is one-order magnitude larger than the new PANS model far from the wall. Furthermore, Figure 4(b)) shows that the new PANS exhibits a real plateau of $f_{k,\text{tar}} = 1$ in the near-wall region, leading to a sharp switch from RANS to LES (at $y^+ \simeq 200$, see insets). On the contrary, the old PANS does not switch to LES at all but stays in RANS mode in the entire channel. For both old and new PANS, the observed f_k is significantly different from the prescribed f_k, see Figure 4(b)). However, for the new PANS, $f_{k,\text{obs}}$ is smaller than $f_{k,\text{tar}}$ everywhere, but the profiles have a quite similar shape.

4.2. Hump flow

The Reynolds number of the hump flow is $Re_c = 936,000$, based on the hump length, $c = 1$, and the inlet mean velocity at the centreline, $U_{\text{in},c}$. In the present simulations, the value of ρ, c and $U_{\text{in},c}$ have been set to unity. The configuration is given in Figure 1. Experiments were conducted by Greenblatt et al. [15, 16]. The maximum height of the hump, h, and the channel height, H, are given by $h/c = 0.128$ and $H/c = 0.91$, respectively. The mesh has $304 \times 108 \times 32$ cells and is taken from the NASA workshop.[2] The spanwise extent is set to $Z_{\text{max}}/c = 0.2$. The inlet is located at $x/c = 0.5$ and the outlet at $x/c = 4.0$.

A periodic boundary condition is applied in the spanwise direction z. Therefore, this direction is considered statistically homogeneous. The inlet conditions (U, V, k and ε) are taken from a 2D RANS simulation using the AKN $k - \varepsilon$ turbulence model [17] coupled to the EARSM model [18]. Synthetic isotropic fluctuations are superimposed on the 2D RANS velocity field. The synthetic fluctuations are scaled with the RANS shear stress profile. To reduce the inlet k, prescribed from 2D RANS, a commutation term $\partial f_k/\partial x$ is used.
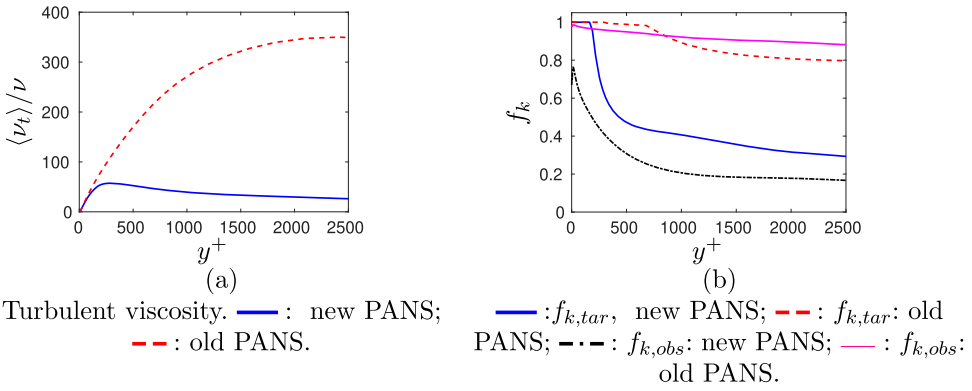
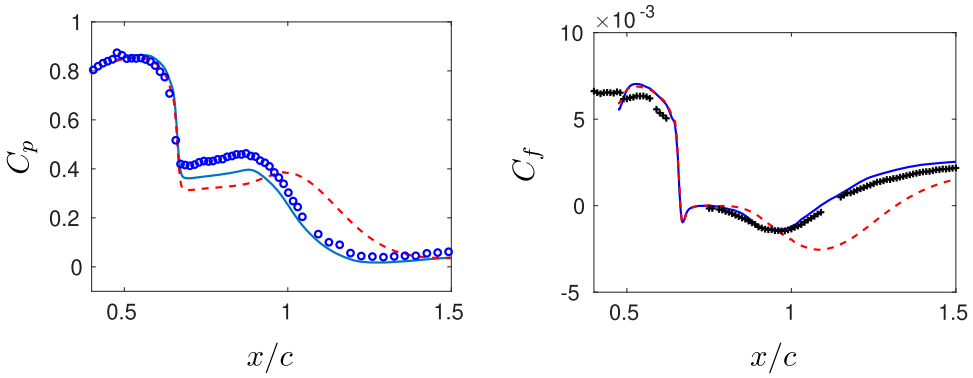**Figure 4.** Channel flow. Viscosity and f_k. $Re_\tau = 5200$.

Figure 5. Hump flow. Pressure coefficient and skinfriction. ——— : new PANS; — — : old PANS; markers: Experiments [15, 16].

For more detail on inlet synthetic fluctuations and the commutation term, see [7]. A lower limit of 0.2 is used when computing f_k from Equation (16).

The simulations are initialised as follows [19]: first the 2D RANS equations are solved. Anisotropic synthetic fluctuations, $(\mathcal{V}'_i)_m$, are then superimposed to the 2D RANS field which gives the initial LES velocity field. In order to compute $(\mathcal{V}'_i)_m$, synthetic fluctuations, $v'_{i,\text{synt}}$, are computed plane-by-plane ($y-z$) in the same way as prescribing inlet boundary conditions. The synthetic fluctuations in the $y-z$ planes are coupled with an asymmetric space filter

$$(\mathcal{V}'_i)_m = a(\mathcal{V}'_i)_{m-1} + b(v'_{\text{synt},i})_m, \tag{21}$$

where m denotes the index of the x_1 location and $a = \exp(-\Delta x_1/L_{\text{int}})$ and Δx_1 and L_{int} denote the grid size and the integral length scale, respectively ($L_{\text{int}} = 0.2$).

Figures 5 and 6 compare predictions with experiments and, as can be seen, the new PANS is in a very good agreement with experiments, while the old PANS exhibits a significant discrepancy at $x/c > 1$. The predicted skinfrictions show a small bump near the inlet, and the reason is (at least partly) that a different RANS turbulence model (EARSM) was
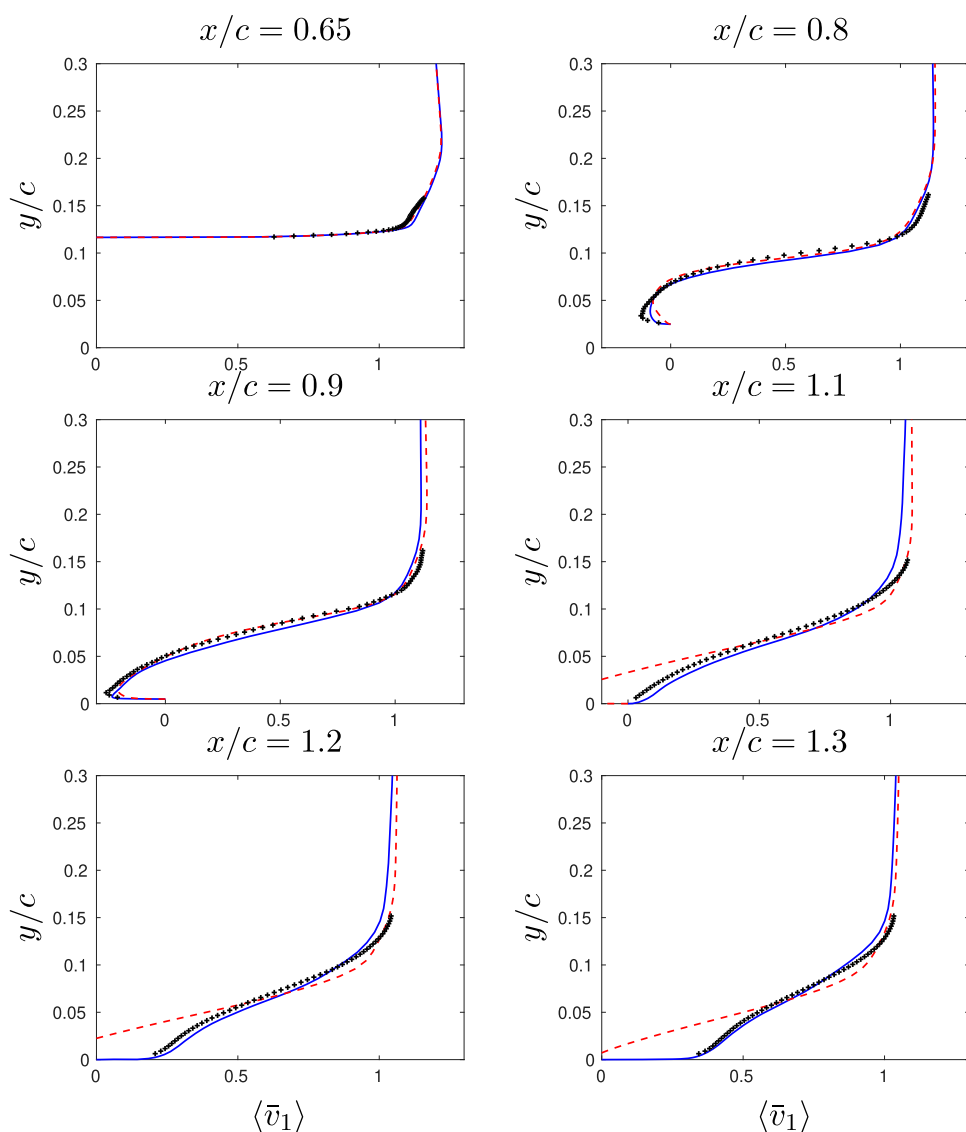
Figure 6. Hump flow. Streamwise velocities. ——— : new PANS; – – – : old PANS; markers: Experiments [15, 16].

used in the 2D RANS simulations than the underlying RANS model in the PANS simulations. The backflow region is well predicted by both PANS models, but globally, the new PANS predicts the streamwise velocity far better than the old PANS.

Figure 7 shows the turbulent viscosity for both models (note that the turbulent viscosities given by the old PANS have been multiplied by 0.1, for the sake of presentation). As in the channel flow, the turbulent viscosities predicted by the old PANS are an order of magnitude larger than those predicted by the new PANS. This means that the solution predicted by the old PANS is closer to RANS than to LES.
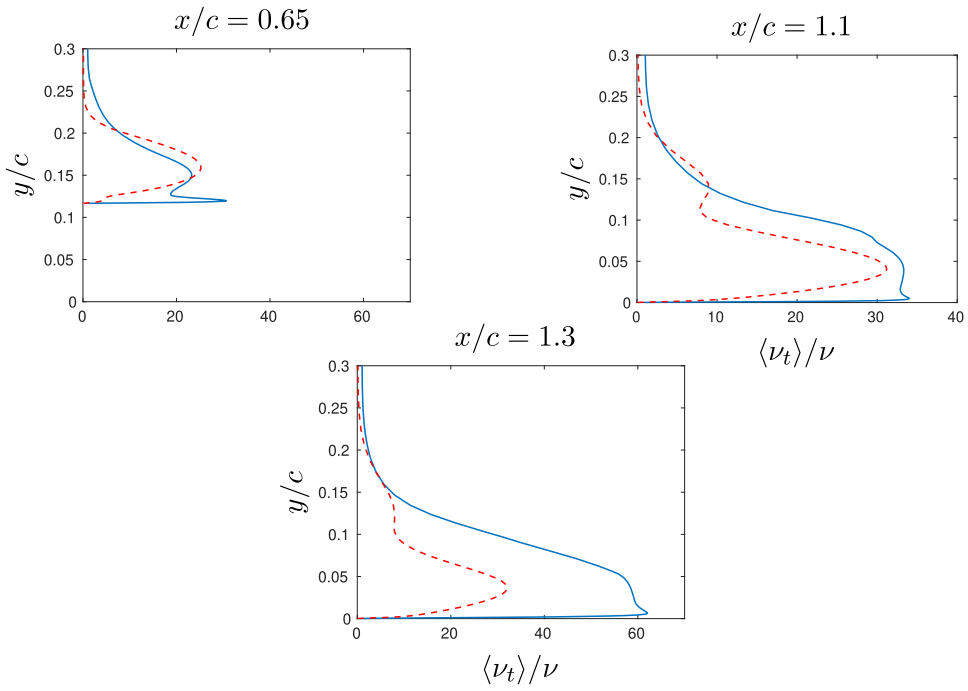
Figure 7. Hump flow. Turbulent viscosity. ——— : new PANS; ‒ ‒ : $0.1\nu_t/\nu$, old PANS.
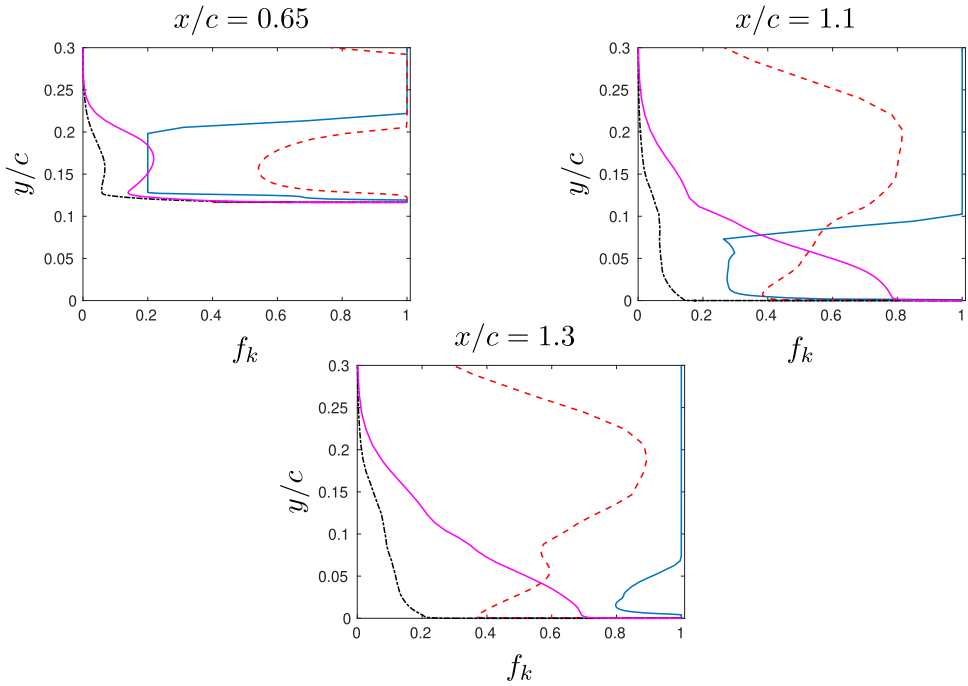

Figure 8. Hump flow. ——— : $f_{k,\text{tar}}$: new PANS; ‒ ‒ : $f_{k,\text{tar}}$: old PANS; — · — : $f_{k,\text{obs}}$: new PANS; ——— : $f_{k,\text{obs}}$: old PANS.
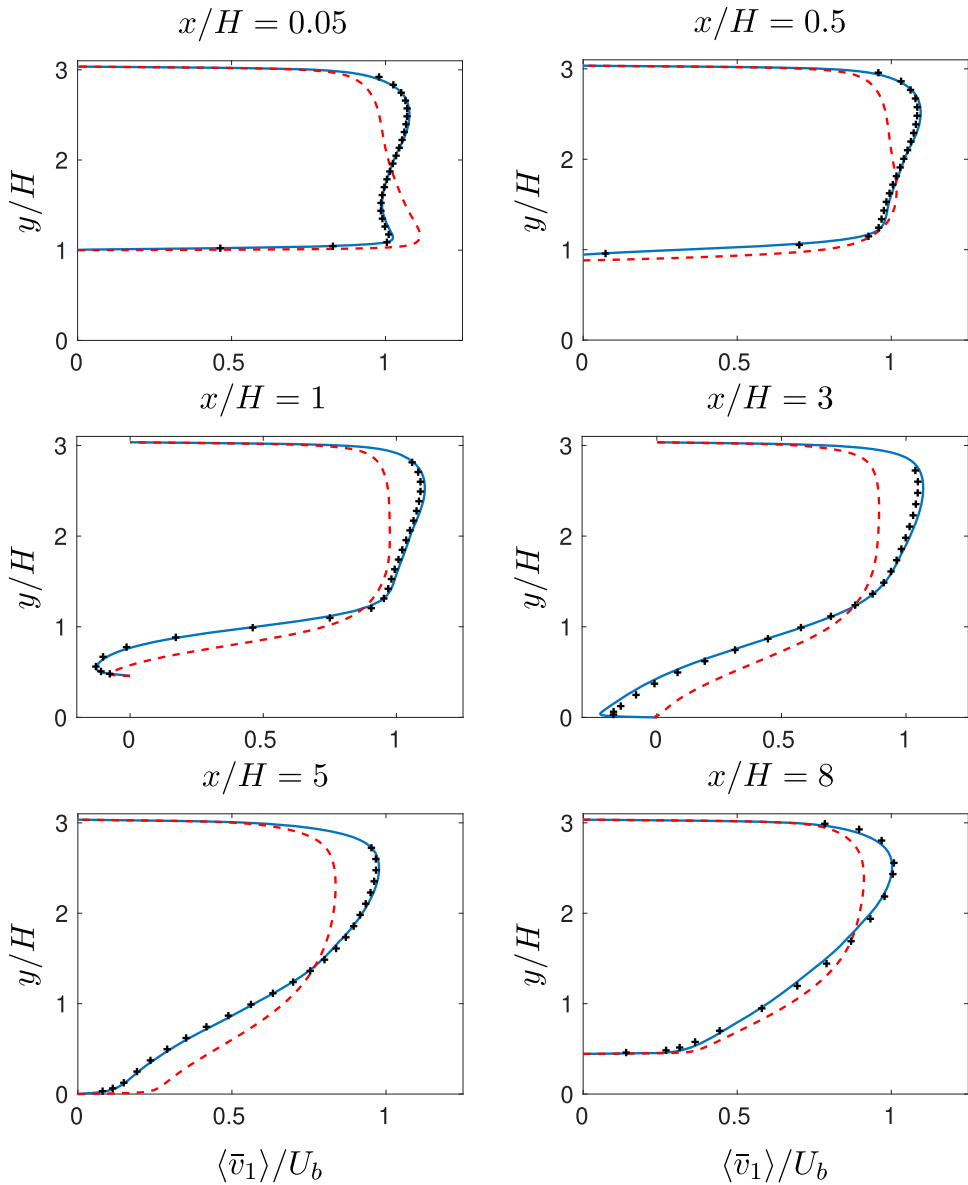
Figure 9. Hill flow. Velocities. ——— : new PANS; ─ ─ : old PANS; markers: LES [22].

Figure 8 presents $f_{k,\mathrm{tar}}$ and $f_{k,\mathrm{obs}}$ for both old and new PANS at three locations, $x/c = 0.65$, 1.1 and 1.3. The old PANS gives a much larger $f_{k,\mathrm{tar}}$ (more RANS) than the new PANS as was noted above in Figure 7. The difference between the two model is largest in the attached flow region. Furthermore, for both approaches, $f_{k,\mathrm{obs}}$ is significantly different from $f_{k,\mathrm{tar}}$, $f_{k,\mathrm{obs}}$ being really low, although the flow is attached to the wall at all three locations. This may be due to the fact that the overall instability of the flow generates a big amount of fluctuations, thus increasing k_{res}, leading to a reduction of $f_{k,\mathrm{obs}}$.
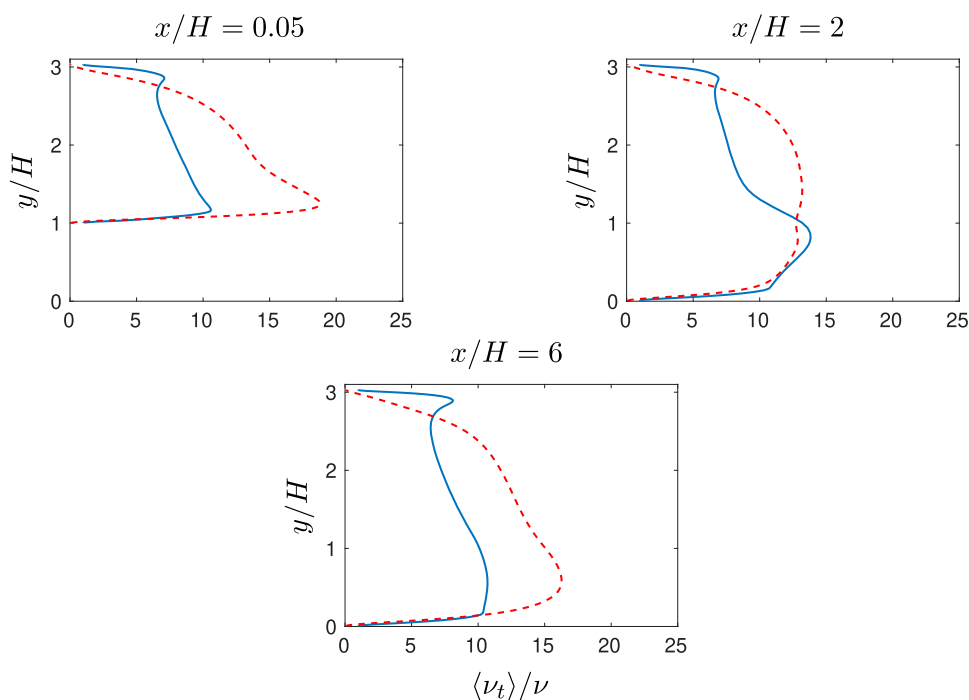
Figure 10. Hill flow. Turbulent viscosities. ——— : new PANS; – – : $0.1\nu_t/\nu$, old PANS.

4.3. Hill flow

The domain is shown in Figure 2. The size of the domain is $9H \times 3.035H \times 4.5H$ in the streamwise (x), wall-normal (y) and span-wise direction (z), respectively. The grid has $160 \times 80 \times 32$ cells in the x, y and z direction. Periodic boundary conditions are used in the x and z directions. The z direction is considered statistically homogeneous. Slip conditions are prescribed at the upper wall. The Reynolds number is $Re = 10,600$ based on the hill height and the bulk velocity at the top of the hill. An initial velocity field is prescribed from a 2D RANS solution with the correct bulk Reynolds number. Furthermore, the same technique for synthetic turbulence as for the hump flow, is used to add initial fluctuations. The bulk velocity is then kept constant by adjusting β in Equation (20) at each time step by ensuring that the sum of the forces at the wall (wall shear stress and pressure on the lower wall) balances the driving pressure gradient [20, 21, Section 4.5]. A lower limit of 0.2 is used when computing f_k from Equation (16).

Figure 9 compares the velocity field with LES of [22] and the agreement with the new PANS model is excellent.However, the old PANS model performs very poorly. The reason for the poor performance of the old PANS is seen in Figure 10 (note that the viscosities of the old PANS have been multiplied by 0.1); the turbulent viscosity is one order of magnitude larger with the old PANS compared to the new PANS.

Figure 11 compares profiles of $f_{k,\text{tar}}$ and $f_{k,\text{obs}}$ for both PANS approaches. It is interesting to notice that at the top of the hill ($x/H = 0.05$), the two $f_{k,\text{tar}}$ are close to each other, while their observed counterparts are significantly different: the new PANS is very well resolved, while the old one is closer to the RANS level. Further downstream, this global tendency is
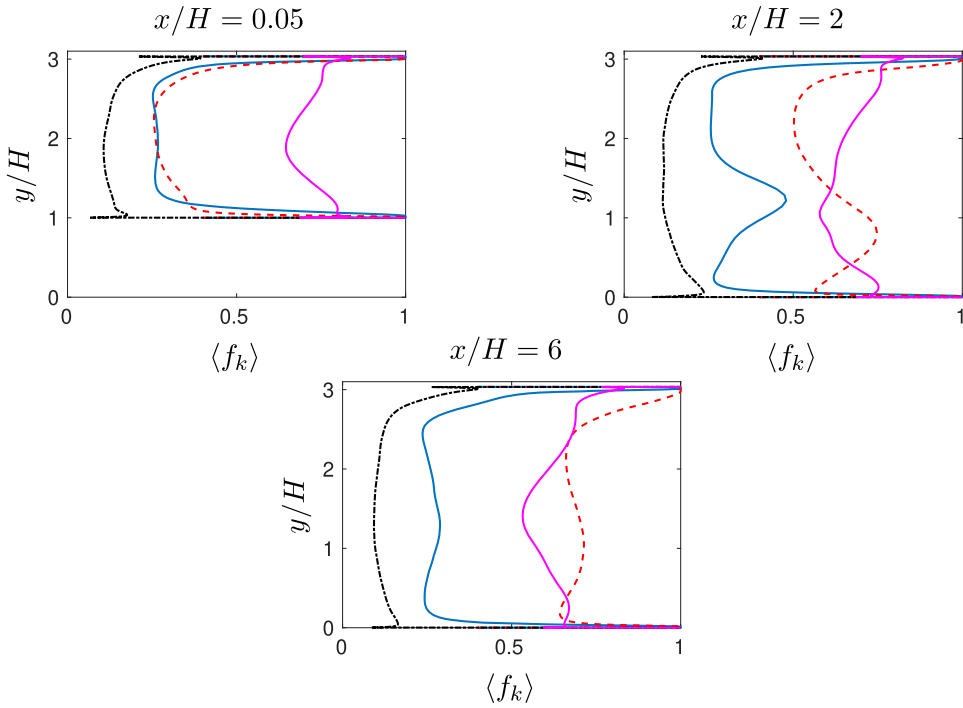
Figure 11. Hill flow. ——— :$f_{k,tar}$, new PANS; – – : $f_{k,tar}$: old PANS; – · – : $f_{k,obs}$: new PANS; ——— : $f_{k,obs}$: old PANS.

conserved, except that old and new PANS stray from each other, even after reattachment ($x/H = 6$).

5. Concluding remarks

A new formulation for prescribing f_k has been presented. It has been found to perform much better than the standard form of f_k of [4, 23]. It should, however, be mentioned that the standard form of f_k works much better when used in a four-equation turbulence model [23] than in a two-equation model as in the present work, presumably because the four-equation closure contains more accurate near-wall physics.

The new formulation presented here, behaves very much like 'classic DES', as one can see in [9], even though they use different mechanisms to separate modelled and resolved scales. In particular, they show very similar performance in separated flows, as well as in attached boundary layers.

Another interesting feature of the new PANS, is the robustness inherited from DES. As explained in Section 2.2, it behaves like a passive control device, in the sense that it does not require the explicit computation of the observed energy ratio $f_{k,obs}$.

So what is the advantage of using PANS instead of DES? One advantage is that PANS has a much stronger theoretical foundation than DES. PANS is rigorously derived whereas DES is an ad-hoc (but very successful) modification of a RANS model. Another advantage of PANS is that the modified partition between modelled and resolved turbulence due to

non-uniform grids can be accounted for by adding a term in the k and momentum equations based on the gradient of f_k [7, 24]. Future work will focus on a thorough theoretical derivation of the relationship between f_k and the grid step, by accounting for inhomogeneity. Another test will consist of prescribing f_k with some more elaborate forms of DES, for instance Improved Delayed Detached Eddy Simulation (IDDES, see e.g. [25, 26]).

Notes

1. ε is independent of f_k provided that no dissipation is resolved, which corresponds to $f_\varepsilon = 1$
2. https://turbmodels.larc.nasa.gov/nasahump_val.html

Disclosure statement

No potential conflict of interest was reported by the authors.

References

[1] Girimaji SS. Partially-averaged Navier-Stokes model for turbulence: a Reynolds-averaged Navier-Stokes to direct numerical simulation bridging method. ASME J Appl Mech. 2006;73(3):413–421.
[2] Schiestel R, Dejoan A. Towards a new partially integrated transport model for coarse grid and unsteady turbulent flow simulations. Theor Comp Fluid Dyn. 2005;18(6):443–468.
[3] Chaouat B, Schiestel R. A new partially integrated transport model for subgrid-scale stresses and dissipation rate for turbulent developing flows. Phys Fluids. 2005;17(065106
[4] Girimaji SS, Abdul-Hamid KS. Partially-averaged Navier-Stokes model for turbulence: implementation and validation. AIAA paper 2005-0502. Reno, NV; 2005.
[5] Kenjeres S, Hanjalic K. LES, T-RANS and hybrid simulations of thermal convection at high ra numbers. Int J Heat Fluid Flow. 2006;27:800–810.
[6] Foroutan H, Yavuzkurt S. A partially-averaged Navier-Stokes model for the simulation of turbulent swirling flow with vortex breakdown. Int J Heat Fluid Flow. 2014;50:402–416.
[7] Davidson L. Zonal PANS: evaluation of different treatments of the RANS-LES interface. J Turbul. 2016;17(3):274–307.
[8] Friess C, Manceau R, Gatski TB. Toward an equivalence criterion for hybrid RANS/LES methods. Int J Heat Fluid Flow. 2015;122:233–246.
[9] Davidson L, Friess C. The PANS and PITM model: a new formulation of f_k. In Proceedings of 12th international ERCOFTAC symposium on engineering turbulence modelling and measurements (ETMM12), Montpelier, i France 26–28 September; 2018.
[10] Ma J, Peng S-H, Davidson L, et al. A low Reynolds number variant of partially-averaged Navier-Stokes model for turbulence. Int J Heat Fluid Flow. 2011;32(3):652–669.
[11] Fadai-Ghotbi A, Friess C, Manceau R, et al. A seamless hybrid rans-les model based on transport equations for the subgrid stresses and elliptic blending. Phys Fluids. 2010;22(5):055104.
[12] Davidson L, Peng S-H. Hybrid LES-RANS: a one-equation SGS model combined with a $k − \omega$ for predicting recirculating flows. Int J Numer Methods Fluids. 2003;43(9):1003–1018.
[13] Emvin P. The full multigrid method applied to turbulent flow in ventilated enclosures using structured and unstructured grids [PhD thesis]. Göteborg: Department of Thermo and Fluid Dynamics, Chalmers University of Technology; 1997.
[14] Lee M, Moser RD. Direct numerical simulation of turbulent channel flow up to $Re_\tau \approx 5200$. J Fluid Mech. 2015;774:395–415. doi:10.1017/jfm.2015.268
[15] Greenblatt D, Paschal KB, Yao C-S, et al. A separation control CFD validation test case. Part 1: baseline & steady suction. AIAA-2004-2220; 2004.
[16] Greenblatt D, Paschal KB, Yao C-S, et al. A separation control CFD validation test case part 1: zero efflux oscillatory blowing. AIAA-2005-0485; 2005.

[17] Abe K, Kondoh T, Nagano Y. A new turbulence model for predicting fluid flow and heat transfer in separating and reattaching flows – 1. Flow field calculations. Int J Heat Mass Transfer. 1994;37(1):139–151. doi:10.1016/0017-9310(94)90168-6

[18] Wallin S, Johansson AV. A new explicit algebraic Reynolds stress model for incompressible and compressible turbulent flows. J Fluid Mech. 2000;403:89–132.

[19] Davidson L. Zonal detached eddy simulation coupled with steady rans in the wall region. In ECCOMAS MSF 2019 thematic confernece, minisyposium 'Current trends in simulation and modelling of turbulent flows. MS devoted to 80th birthday of Prof. Kemo Hanjalic'. September 18th–20th, 2019 – Sarajevo, Bosnia and Herzegovina; 2019.

[20] Irannezhad M. DNS of channel flow with finite difference method on a staggered grid [Msc thesis]. Göteborg: Division of Fluid Dynamics, Department of Applied Mechanics, Chalmers University of Technology; 2006.

[21] Orlandi P. Fluid flow phenomena – a numerical toolkit. Dordrecht: Kluwer Academic Publishers; 2000.

[22] Breuer M, Peller N, Rapp C, et al. Flow over periodic hills – numerical and experimental study in a wide range of Reynolds numbers. Comput Fluids. 2009;38:433–457. doi:10.1016/j.compfluid.2008.05.002

[23] Basara B, Krajnović S, Girimaji S, et al. Near-wall formulation of the partially averaged Navier Stokes turbulence model. AIAA J. 2011;49(12):2627–2636.

[24] Girimaji SS, Wallin S. Closure modeling in bridging regions of variable-resolution (VR) turbulence computations. J Turbul. 2013;14(1):72–98. doi:10.1080/14685248.2012.754893

[25] Shur ML, Spalart PR, Strelets MK, et al. A hybrid rans-les approach with delayed-des and wall-modelled les capabilities. Int J Heat Fluid Flow. 2008;29(6):1638–1649.

[26] Gritskevich MS, Garbaruk AV, Schütze J, et al. Development of ddes and iddes formulations for the k-ω shear stress transport model. Flow Turbul Combust. 2012;88(3):431–449.